24th COBEM - 2017

24th ABCM International Congress of Mechanical Engineering
December 3-8, 2017, Curitiba, PR, Brazil

COBEM-2017-2138
HYDROELASTIC EFFECTS IN STRUCTURAL RESPONSE UNDER WAVE IMPACT

Rubens Augusto Amaro Junior
Liang-Yee Cheng
Department of Construction Engineering, Polytechnic School of University of São Paulo
Av. Prof. Almeida Prado, trav. 2, 83 - Cidade Universitária, 05508-900, São Paulo, SP, Brazil
rubens.amaro@usp.br
cheng.yee@usp.br

Abstract. *Hydroelastic phenomena involving flexible bodies and free surface flow are important for several engineering applications and have received considerable attention in different fields. Some examples are: the dynamics of very large floating structures (floating airport, bridge, etc.) interacting with water waves, internal structures responses of liquid storage tanks, efficiency of wave energy converters, etc. A potentially important parameter in modeling hydroelasticity is the stiffness of the flexible body. If the body is elastic then liquid and structural motions can couple and drastically alter the structure response and the hydrodynamic loads. In this work, the influence of stiffness of the flexible body subject to a wave impact is investigated by using the Lagrangian particle-based method Moving Particle Simulation (MPS). It is a meshless method used to model both fluid and elastic solid, where the entire computational domain is discretized in particles. In case of fluid-structure interaction, a partitioned coupling between fluid and isotropic elastic solid is adopted. Explicit and semi-implicit time integration algorithms are used for elastic solid and fluid domains, respectively. To validate the numerical model, quantitative comparisons with available numerical results of dam breaking flow hitting an elastic plate are performed. Then the effects of the stiffness on the hydrodynamic load and structural response are investigated based on the dam breaking problem.*

Keywords: *hydroelasticity, wave impact, fluid-structure interaction, particle method, MPS*

1. INTRODUCTION

Hydroelastic engineering problems has attracted increasing interest due to wide range of its application in several areas. Some interesting examples are: the dynamics of very large floating structures (floating airport, bridge, etc.) interacting with water waves (Wang and Tay, 2011), internal structures responses of liquid storage tanks (Miras *et al.*, 2012), efficiency of wave energy converters (Chaplin *et al.*, 2012), etc. A potentially important parameter in modeling hydroelasticity is the stiffness of the flexible body. If the body is elastic then liquid and structural motions can couple and drastically alter the structure response and the hydrodynamic loads. The investigation of the wave impact on a rigid and elastic wall was previous investigated experimentally and numerically by some authors (Wemmenhove *et al.*, 2010; Mai *et al.*, 2015) as well as the sloshing phenomenon within rigid and elastic tanks (Choi *et al.*, 2012; Lugni *et al.*, 2013; Tang *et al.*, 2016). In this work, hydrodynamic load and structure dynamic response, for different stiffness of the flexible body, subject to a wave impact are investigated by using the particle-based method Moving Particle Simulation (MPS) (Koshizuka and Oka, 1996), formerly called as Moving Particle Semi-implicit.

In general, as a Lagrangian meshless method, the MPS is very effective for the simulation of hydrodynamics problems involving free surface, fragmentation and merging, and problems involving large deformation, complex shaped bodies and moving boundaries. The method can be used to model both fluid and elastic solid (Chikazawa *et al.*, 2001; Song *et al.*, 2001; Amaro Jr and Cheng, 2013), so that the entire computational domain is discretized in particles. In case of fluid-structure interaction, a partitioned coupling between fluid and isotropic elastic solid is adopted. Explicit and semi-implicit time integration algorithms are used for elastic solid and fluid domains, respectively. Matching of the time steps in both domains is done by subcycling technique to improve the computational efficiency.

The verification and performance of the method are evaluated by analyzing the results of dam breaking on an elastic plate. At first, the horizontal displacement of the top of the elastic plate are compared with available numerical results (Walhorn *et al.*, 2005; Marti *et al.*, 2006; Idelsohn *et al.*, 2008; Amanifard *et al.*, 2011). After that, the effects of different stiffness on the hydrodynamic load and structural response of the elastic plate are investigated using the dam breaking problem. Pressure time series, pressure impulses and displacements computed for six stiffness, one of which is rigid, are investigated and compared.

2. COMPUTATIONAL PROCEDURE

Moving Particle Simulation (MPS) method is a fully Lagrangian meshfree particle-based approach. Originally proposed by Koshizuka and Oka (1996) for the simulation of incompressible flow with free surface, initially it adopts a semi-implicit algorithm to solve the governing equations of continuum by replacing the differential operators with numeric operators derived from a particle interaction model based on a weight function.

To solve the incompressible viscous flow, a semi-implicit algorithm is used in the MPS method. At first, predictions of the particle's velocity and position are carried out explicitly by using viscosity and external forces terms of the momentum conservation. The pressure of all particles is calculated by the Poisson equation for the pressure, which is solved implicitly. The RHS term of the Poisson equation is proportional to the deviation of particle number density from its initial value (zero variation of density condition), which is a parameter that is proportional to the density of the fluid in the vicinity of the particle. Then the velocity of the particles is updated by using the pressure gradient term of the momentum conservation and the new positions of the particles are obtained.

For elastic solid, an explicit algorithm is used in the MPS method solid (Chikazawa *et al.*, 2001; Song *et al.*, 2001). First, the displacement vector between particles and its neighbor is calculated and the strain vectors are computed. From the strain vectors, the stress tensor can be obtained and by using the governing equations of elastic solids, the particle's velocity and position are carried out explicitly.

Solid wall boundary condition is imposed by using three layers of fixed particles. The particles that from the layer in contact to the fluid are denominated wall particles, of which the pressure is computed by solving Poisson equation for the pressure, together with the fluid particles. The particles that form two other layers are denominated dummy particles. Dummy particles are used to assure the correct calculation of the particle number density of the wall particles. Pressure is not calculated in the dummy particles.

In order to improve the precision and stability of the fluid computation, Neighborhood Particles Centroid Deviation condition (Tsukamoto *et al.*, 2016) is used in the present work to identify the free-surface particles. A particle is defined as free-surface particle and its pressure is set to zero when its particle number density is smaller than initial value of the particle number density multiplied by a threshold value, and the magnitude of the weighted average deviation is greater than initial particle distance multiplied by a threshold constant.

A partitioned weak coupling algorithm is adopted for the fluid-structure interaction. The elastic solid surface particles are treated like a fluid particle and the pressures of the elastic solid surface particles are computed by solving Poisson equation for the pressure, together with the fluid particles. Therefore, the coupling between solid and fluid is done at first by using the displacement and velocity of elastic solid as the boundary conditions for the fluid domain. Then the pressure on the elastic solid surface particles is obtained by solving the fluid motion. After that the force obtained from the integration of the pressure on the elastic solid surface is taken into account in the calculation of the motion of the elastic solid. Matching of the time steps in both domains is done by sub-cycling technique to improve the computational efficiency. More detailed description of the MPS method, can be found in (Koshizuka and Oka, 1996) and in the previous work of the authors (Amaro Jr and Cheng, 2013).

2.1 Fluid-structure interaction

In this work, in relation to the previous work (Amaro Jr and Cheng, 2013), improvements have been made on the calculation of the elastic solid surface normal vector and integration of pressure on the elastic solid. The obtained hydrodynamic loads are taken into account in the calculation of the motion and deformation of the elastic solid. Focusing the impulsive hydrodynamic loads on the elastic solid, shear forces were neglected and the force is calculated as

$$\vec{f}_i = -\iint_{Si} P_i d\vec{S} = -P_i l_0^d \vec{n}_i , \tag{1}$$

where P_i is the pressure on the elastic solid surface particle *i*, the vector $d\vec{S}$ denotes the area multiplied by the normal vector on the elastic solid surface, l_o^d symbolizes the initial distance between two adjacent particles raised to the number of space dimensions d (2 for bi-dimensional and 3 for three-dimensional) and $\vec{n}_i$ represents the normal vector of the elastic solid surface particle *i*.

After the deformation of the elastic solid, the normal vector $\vec{n}_{i,t}$ at the time step *t* is updated as

$$\vec{n}_{i,t} = \left(\nabla \vec{r}_{ij,t}\right)^{-T} \vec{n}_{i,0} , \tag{2}$$

where deformation gradient tensor $\nabla \vec{r}_{ij,t}$ is calculated by the gradient operator of MPS

$$\nabla \vec{r}_{ij,t} = \left\langle \nabla \vec{r}_{ij,t} \right\rangle_i = \sum_{j=1}^{Neigh} \vec{r}_{ij,t} \otimes \vec{r}_{ij,0} A_i^{-1}, \tag{3}$$

$$A_i = \sum_{j=1}^{Neigh} \vec{r}_{ij,0} \otimes \vec{r}_{ij,0}\,, \tag{4}$$

where $\vec{r}_{ij,t}$ and $\vec{r}_{ij,0}$ are the differences between the position vectors of the particle *i* and its neighbor *j* at the time step *t*, and the initial state, respectively.

The initial normal vector of the elastic solid $\vec{n}_{i,0}$, in each particle, is obtained as summations of the coordinate deviation between the particle and its neighborhood particles for each direction of Cartesian space, divided by its norm

$$n_x = -\sum_{j=1}^{Neigh} x_j - x_i\,,\; n_y = -\sum_{j=1}^{Neigh} y_j - y_i\,,\; n_z = -\sum_{j=1}^{Neigh} z_j - z_i\,, \tag{5}$$

$$\vec{n}_{i,o} = -\frac{1}{\left\| n_x^2 + n_y^2 + n_z^2 \right\|} \left(n_x, n_y, n_z \right). \tag{6}$$

3. RESULTS AND DISCUSSION

3.1 Verification of numerical method

A dam breaking problem with a fixed elastic plate is simulated, allowing the investigation of interaction between fluid and elastic solid. The lower end of the elastic plate is clamped to the rigid boundary, while the remain part is released at the beginning of the simulation and is free to move. The initial configuration of the problem is shown in Fig 1. The dimensions of elastic plate, which is highlighted in orange color, are 12.0 mm thick and 80.0 mm long. The physical properties of the elastic solid, fluid and simulation parameters are presented in Tab. 1. For all cases analyzed herein, the effective radius r_e is set to $2.1l_0$ to compute the gradient and divergence operators and the particle number density, where l_0 signifies the initial distance between two adjacent particles. The effective radius r_e is set to $4.0l_0$ to compute the Laplacian operator. The simulation is performed for 2 s.

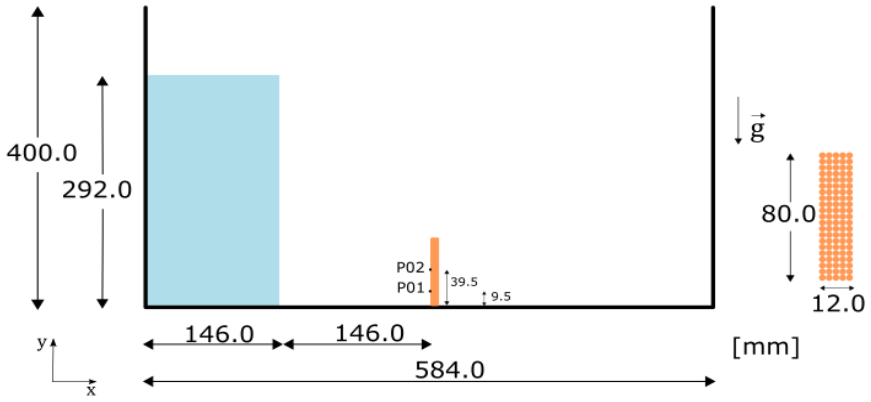

Figure 1. Dam breaking flow hitting a vertical elastic plate. Dimensions.

Table 1. Dam breaking flow hitting a vertical elastic plate. Physical properties and simulation parameters.

Parameter	Elastic Solid	Parameter	Fluid
Time step (s)	10^{-6}	Time step (s)	$2x10^{-5}$
Particle distance (m)	0.001	Particle distance (m)	0.001
Density (kg/m^3)	2500	Density (kg/m^3)	1000
Young's modulus (Pa)	10^6	Kinematic viscosity (m^2/s)	10^{-6}
Poisson's ratio	0.0		

Figure 2 shows a sequence of frames from the simulation obtained by Smoothed Particle Hydrodynamics (SPH) (Rafiee and Thiagarajan, 2009), Particle Finite Element Method (PFEM) (Idelsohn *et al.*, 2008) and the simulations carried in the present study. The colors on the fluid of PFEM and MPS cases are associated to pressure field. The pressure field is not showed on the fluid of SPH. The pressure field, the shape of the deformation of the elastic beam as well as the free surface perturbation seems to be in a good agreement with the SPH and PFEM methods.

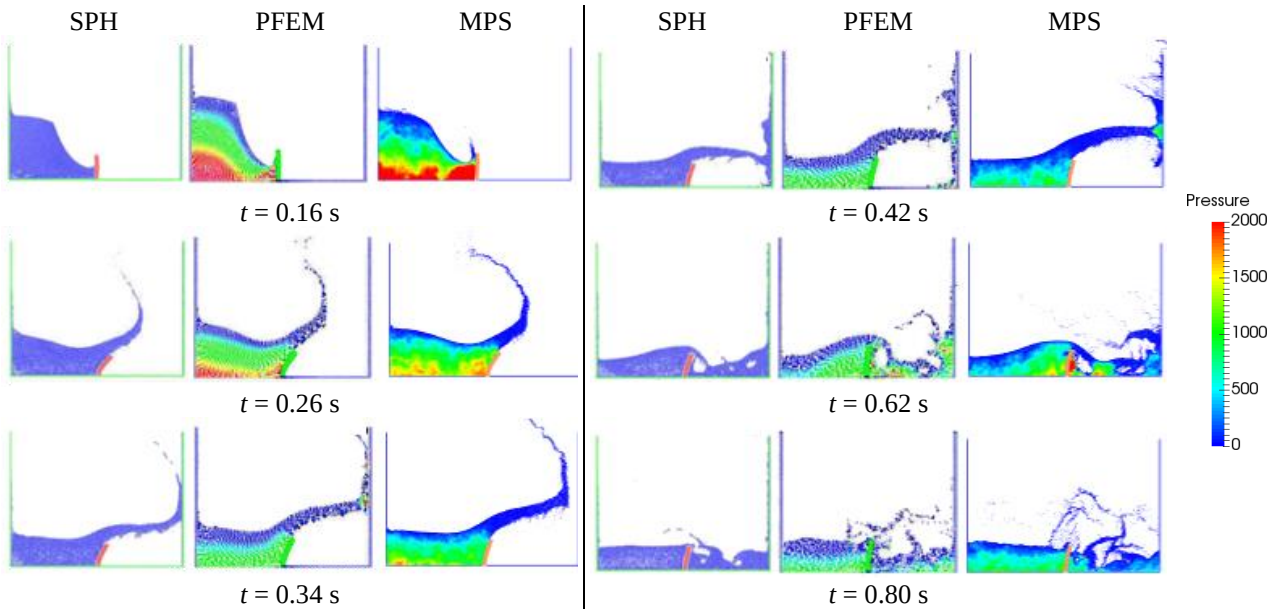

Figure 2. Comparison between SPH (Rafiee and Thiagarajan, 2009), PFEM (Idelsohn et al., 2008) and present MPS at the instants: 0.16 s, 0.26 s, 0.34 s, 0.42 s, 0.62 s and 0.80 s.

Figure 3 shows the time history of the horizontal displacement of the top of the elastic plate obtained by the present simulation and the numerical results available in the literature, computed by Finite Element Method (FEM) (Walhorn *et al.*, 2005), PFEM (Marti *et al.*, 2006; Idelsohn *et al.*, 2008) and SPH (Amanifard *et al.*, 2011). Comparing the result obtained by MPS simulation with other methods, it may be noted that initially the MPS results has the same tendency as the other ones. However, a maximum displacement of 0.039 m is close to that obtained by FEM and SPH, and slightly lower than the results from PFEM computations. After the instant t = 0.4 s the displacement obtained by the present simulation remains in 0.015 m, which is in the same order to the results of PFEM and SPH simulations. From t = 0.6 s, each numerical method exhibits distinct oscillating behavior. In addition to this, the oscillations tend to a point of equilibrium due to the damping between fluid and elastic plate motion, after the instant t = 1.5 s.

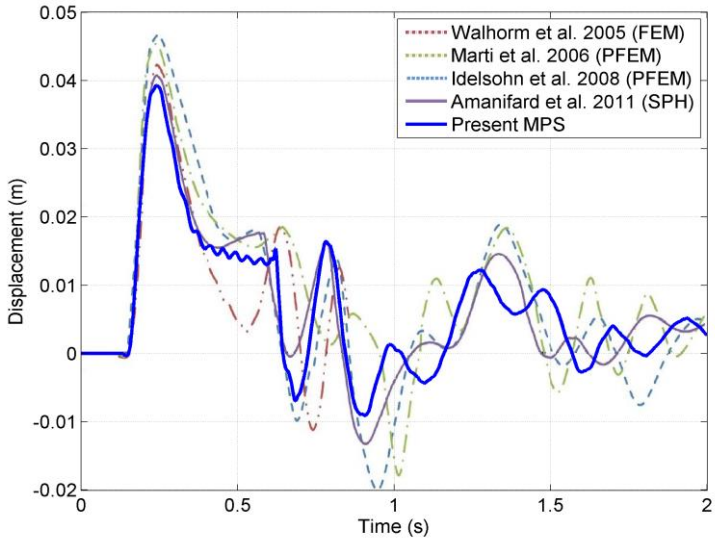

Figure 3. Horizontal displacement of the top of the elastic plate.

3.2 Different values of stiffness

Finally, the dam breaking problem is simulated with different values of stiffness, and the pressure time series are computed at positions P01 (height 9.5 mm) and P02 (height 39.5 mm) (see Fig. 1), allowing the investigation of the influence of the stiffness on the structural response and hydrodynamic loads. The physical properties of the elastic solid, fluid and simulation parameters are presented in Tab. 2. The same values of effective radius r_e adopted in the previous case are used here.

Table 2. Dam breaking with different values of stiffness. Physical properties and simulation parameters.

Parameter	Elastic Solid					Parameter	Fluid
Time step (s)	10^{-6}	$5x10^{-7}$		$5x10^{-8}$		Time step (s)	$2x10^{-5}$
Young's modulus (Pa)	$2x10^{7}$	$2x10^{8}$	$2x10^{9}$	$2x10^{10}$	$2x10^{11}$		
Particle distance (m)	0.001					Particle distance (m)	0.001
Density (kg/m^3)	7800					Density (kg/m^3)	1000
Poisson's ratio	0.3					Kinematic viscosity (m^2/s)	10^{-6}

The raw pressure time series, their single-sided amplitude spectrum and the filtered pressure computed at position P01 for the elastic plate with E = 20 MPa and the rigid plate are illustrated in Fig. 4 and Fig. 5, respectively. Pressure time series are non-dimensionalized with regards to the initial hydrostatic pressure $C_p = P/(\rho g H)$ and are plotted versus the non-dimensional time $\tau = t(g/H)^{0.5}$, where g = 9.81 m/s^2 is the gravitational acceleration and H = 0.292 m denotes the initial water column. It is observed from Figs. 4 (b) and 5 (b) that the energy of the spectrum of pressure are mainly concentrated for frequencies lower than 30 Hz, approximately. Rigorously, ensuring the significative range of frequencies for the hydrodynamic impact, we adopt a cut-off frequency of Fc = 70Hz and a low-pass filter is applied on the pressure time series, avoiding high frequency noise.

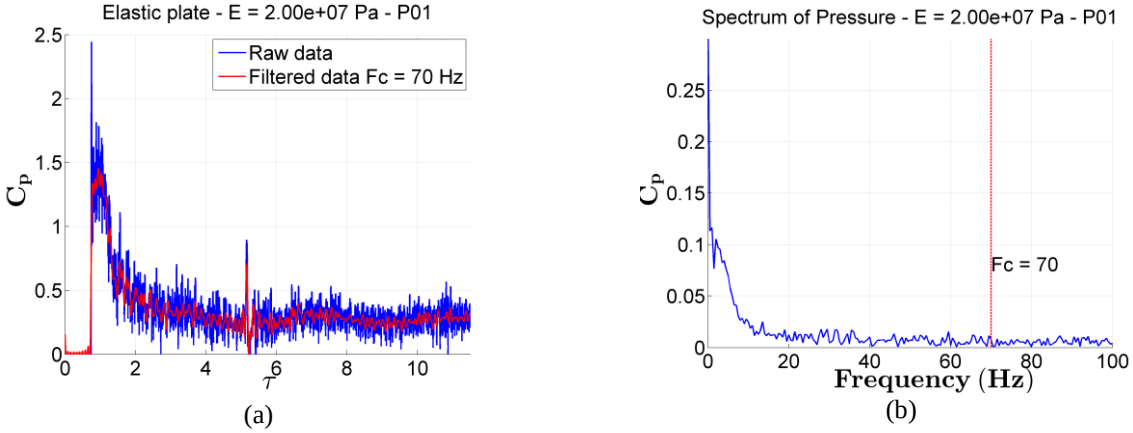

Figure 4. (a) Raw and filtered pressure time series at position P01. (b) Single-sided amplitude spectrum of the raw pressure time series. Elastic plate with E = 20 MPa.

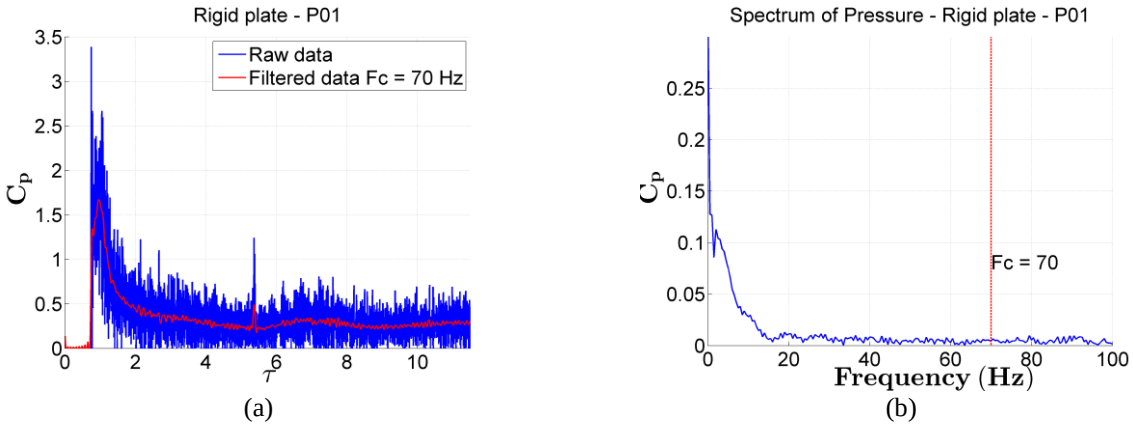

Figure 5. (a) Raw and filtered pressure time series at position P01. (b) Single-sided amplitude spectrum of the raw pressure time series. Rigid plate.

The low-pass filtered pressure time series computed at positions P01 and P02 are presented in Figs. 6 and 7, respectively.

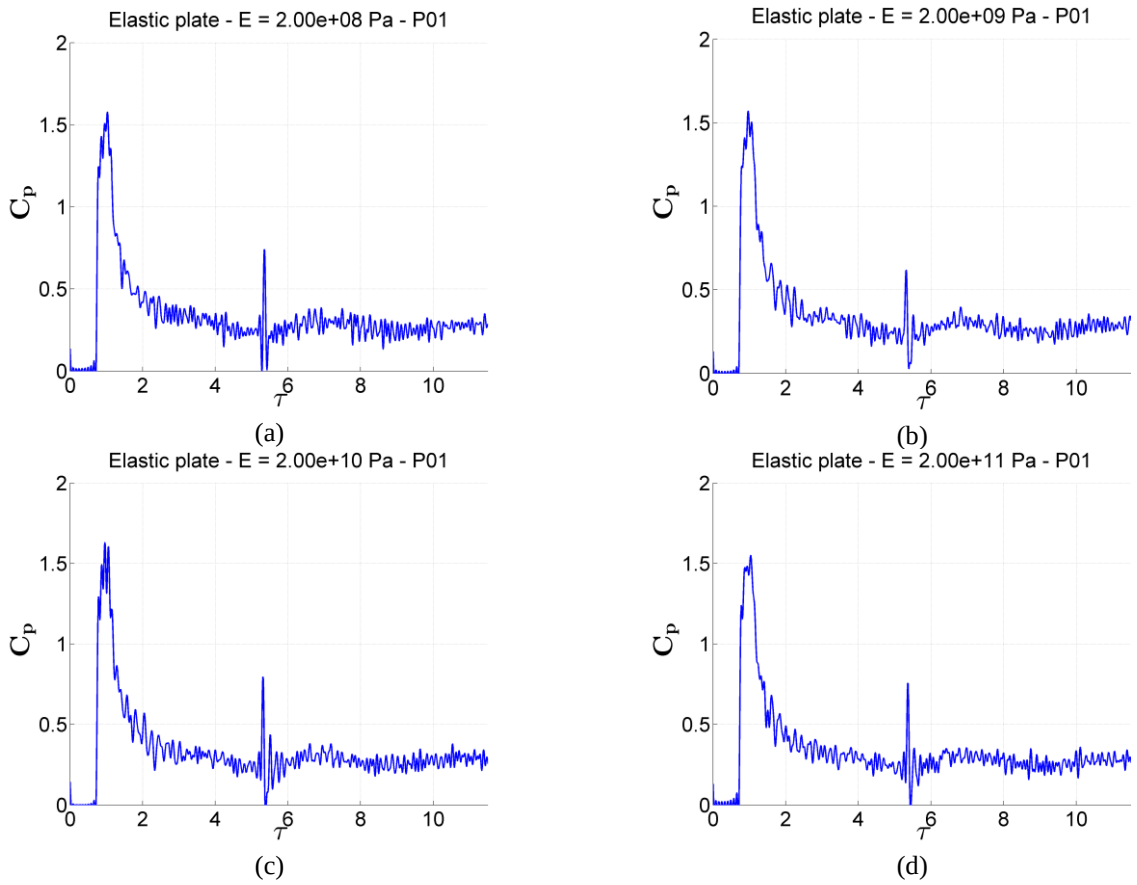

Figure 6. Filtered pressure time series at position P01. Elastic plate with Young's modulus of (a) 200 MPa, (b) 2 GPa, (c) 20 GPa and (d) 200 GPa.

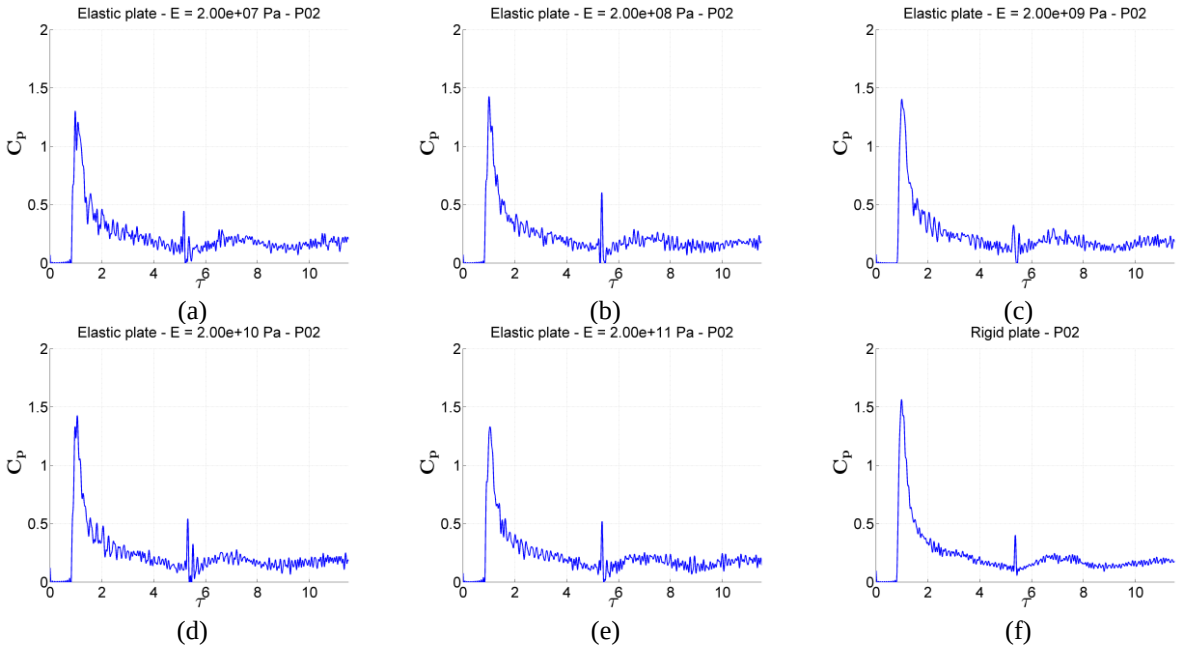

Figure 7. Filtered pressure time series at position P02. Elastic plate with Young's modulus of (a) 20 MPa, (b) 200 MPa, (c) 2 GPa, (d) 20 GPa, (e) 200 GPa and (f) rigid plate.

Considering the pressure at position P01, the wave impacts on the elastic plates produce non-dimensional peak pressures between 1.45 and 1.63, whereas a high peak pressure of 1.67 is computed in the rigid plate, as can be observed from Fig. 6. A lower second non-dimensional peak pressure (values between 0.50 and 0.80) occurs approximately at the non-dimensional time of τ = 5.5, due the collapse of the upward water flow subjected to gravity. After the second pressure peak, a similar pattern is computed for all the cases, with a non-dimensional pressure oscillating around C_p = 0.30.

From Fig. 7, the non-dimensional peak pressures at position P02 are in the range between 1.30 and 1.42 for the elastic plate, whereas the high peak pressure computed in the rigid plate is C_p = 1.57. As shown in the pressure time series at position P01, the collapse of the upward water flow subjected to gravity leads to a second non-dimensional peak pressure of values between 0.33 and 0.60. A non-dimensional pressure oscillating around 0.17 is computed for all the cases, after the second peak pressure.

In the pressure time histories of the very short hydrodynamic impact phenomenon, the position P01 presents a relative difference of 15.17% between the maximum peak pressure of 1.67 (rigid plate) and the minimum of 1.45 (elastic plate with E = 20 MPa), whereas the position P02 presents the difference of 20.77% between the maximum peak of 1.57 (rigid plate) and the minimum peak 1.30 (elastic plate with E = 20 MPa). The relative difference R is defined herein as

$$R = \frac{\max value - \min value}{\min value}. \tag{7}$$

The analysis is also performed considering non-dimensional pressure impulse. In the present work, the non-dimensional pressure impulse is calculated as the integral of the pressure over the duration of the non-dimensional time τ = 11.59 (2 seconds)

$$C_I = \int_0^{11.59} C_p d\tau . \tag{8}$$

The non-dimensional pressure impulse as function of Young's modulus, at positions P01 and P02, are respectively illustrated in Fig. 8 (a) and Fig. 8 (b). The value of the non-dimensional pressure impulse on the rigid plate is represented by a blue solid line, which is C_I = 3.88 at the position P01 and C_I = 2.58 at the position P02.

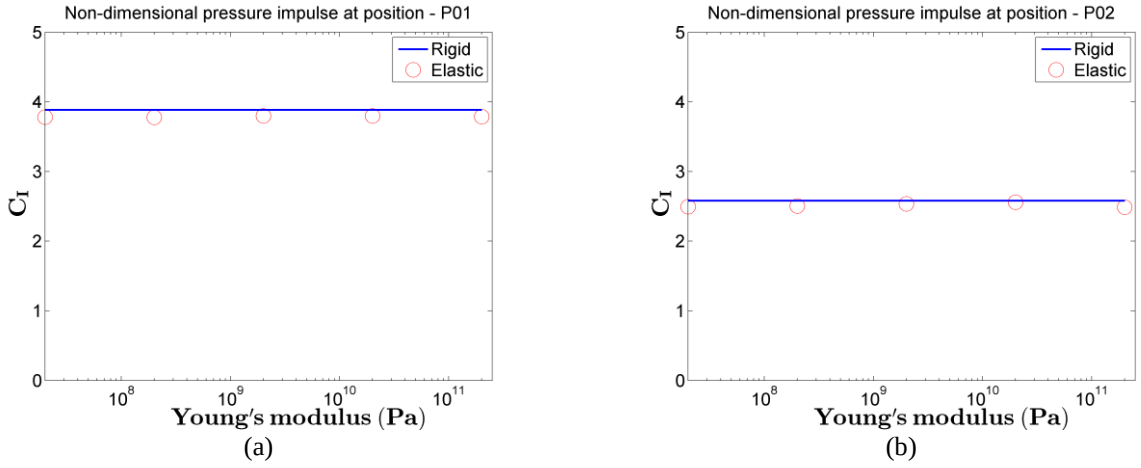

Figure 8. Non-dimensional pressure impulse at (a) position P01 and (b) position P02.

The computed results show that the elastic plates present values between 3.78 and 3.80, whereas the rigid plate presents a non-dimensional pressure impulse of 3.88 for the pressure computed at position P01. For the position P02, non-dimensional pressure impulse of the elastic plates ranges from 2.49 to 2.56, whereas the rigid plate presents a non-dimensional pressure impulse of 2.58. The relative differences between the maximum and minimum values of the non-dimensional pressure impulses are 2.65% for the position P01 and 3.61% for the position P02.

Despite small differences between pressure impulses, 2.65% and 3.61%, these differences are not substantial and, considering all time of impact, the influence of the stiffness on the hydrodynamic loads can be neglected. However, the relative differences of the non-dimensional peak pressures of 15.17% and 20.77% indicate that very short hydrodynamic impact phenomenon is dependent of the stiffness of the structure. Thus, the correctly modelling of the structure physical properties is recommended for particular cases mainly focused on very short time events.

Figure 9 gives the time history of the horizontal displacements and their maximums at the top of the elastic plate obtained for the different stiffness. Displacement time series are non-dimensionalized with regards to the plate thickness e = 0.012 m. The fluid impact on the flexible wall leads to a maximum horizontal displacement up to about 35% of the plate thickness. After initial impact load, the elastic plate moves back and forth, gradually decreasing the excitation amplitude due to damping effects. It can be observed in Fig. 9 (b) that elastic plates with Young's modulus higher than $2x10^9$ Pa (2 GPa) has the maximum horizontal displacement lower than 0.5% of the plate thickness, close to the fixed rigid plate.

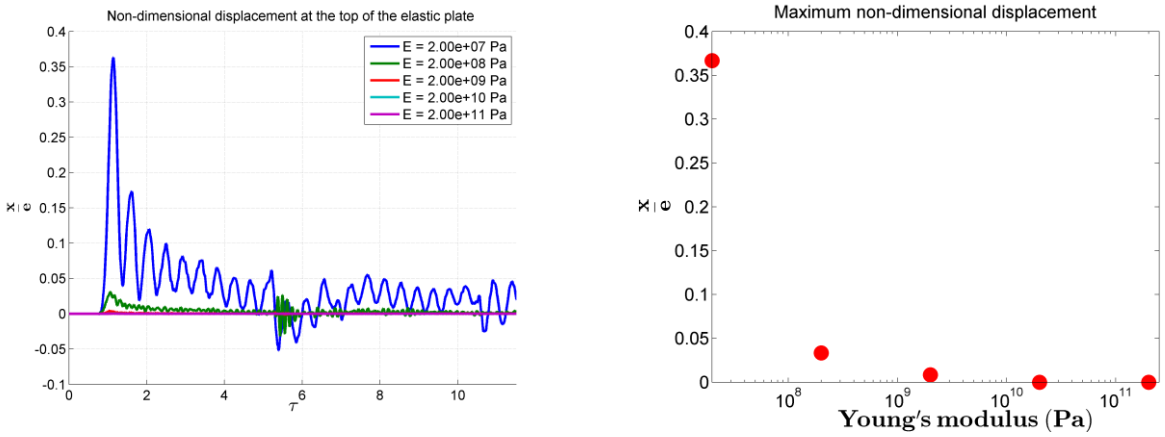

(a) (b)

Figure 9. (a) Non-dimensional horizontal displacement time series and their (b) maximums at the top of the elastic plate for different stiffness.

Figure 10 illustrates snapshots of the fluid, elastic and rigid plates obtained by the present method. The colors on the fluid are associated to the non-dimensional velocity field $C_v = |v|/(gH)^{0,5}$. The fluid impacts the plate with a high velocity at the instant τ = 0.81. At the instant τ = 2.43, the fluid overtops the plate and hit the right tank wall. At the instant τ = 3.13, the upward water flow falls due to gravity and the fluid inside the gap between the plate and the right tank wall presents a complex flow pattern. It can be observed a similar behavior of the velocity field, the shape of the deformation of the elastic beam as well as the free surface perturbation between the simulations.

4. CONCLUSIONS

In the present work, a Lagrangian particle-based numerical technique for the modeling and simulation of fluid-structure interaction problems is shown. A partitioned weak coupling algorithm is used allowing exchange of information between different physical domains. A sub-cycling algorithm of elastic solid is adopted during the simulation to avoid the use of very small time step for both fluid and solid domain in order to reduce the computational cost. Simulations are carried out comparing the results from present simulation with the available numerical results. The computed horizontal displacement obtained by the present method is in a good agreement with the results obtained by another methods. The pressure field as well as the free surface perturbation seems to be in a good agreement with the SPH and PFEM methods, taking into account the physics of the problem. Concerning the case of dam breaking with different values of stiffness, the simulation results show that the peak pressures computed in the rigid plate is higher than the peak pressures in elastic plates. Relative differences of 15.17% and 20.77%, between the maximum and minimum non-dimensional peak pressures, are obtained at positions P01 (height 9.5 mm) and P02 (height 39.5 mm), respectively. However, the differences between the maximum and minimum non-dimensional pressure impulses are almost negligible, with values of 2.65% and 3.61% respectively at positions P01 and P02. Finally, the horizontal displacement of the elastic plates with Young's modulus higher than $2x10^9$ Pa (2 GPa) has the maximum horizontal displacement lower than 0.5% of the plate thickness, close to the fixed rigid plate.

5. ACKNOWLEDGEMENTS

This work was supported by CAPES and the authors are grateful to Petrobras for financial support on the development of the MPS/TPN/USP simulation system based on MPS method.

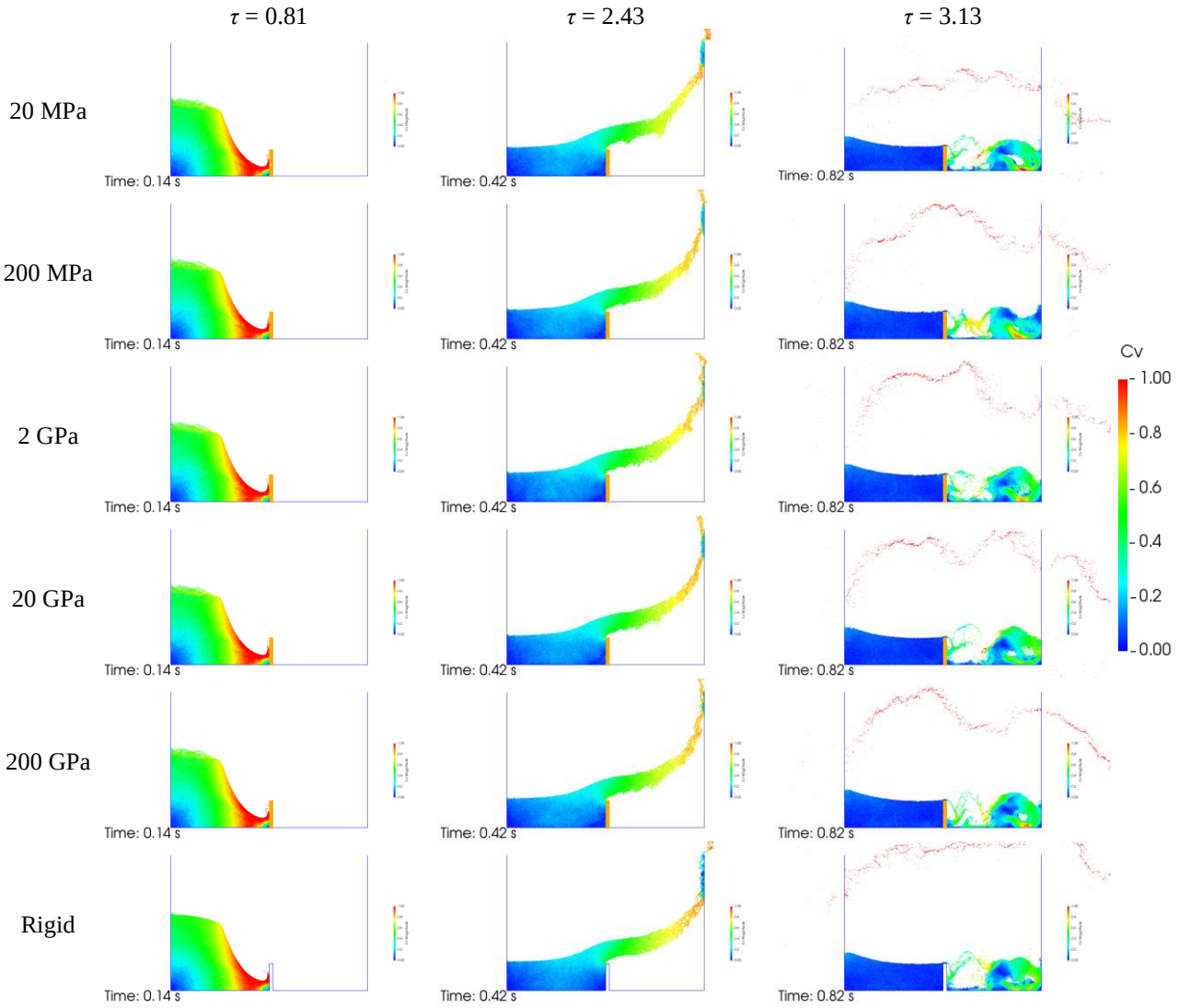

Figure 10. Snapshots of the simulations. Elastic plate with Young's modulus of 20 MPa, 200 MPa, 2 GPa, 20 GPa, 200 GPa and rigid plate.

6. REFERENCES

Amanifard, N., Hesan, M. and Rahbar, B., 2011. "An SPH approach for fluid-hypoelastic structure interactions with free surfaces". In *Proceedings of the World Congress on Engineering – WCE2011*. London, U.K.

Amaro Jr, R.A. and Cheng, L.-Y., 2013. "Brittle fracture and hydroelastic simulations based on moving particle simulation". *Computer Modeling in Engineering & Sciences*, Vol. 2, pp. 87-118.

Chaplin, J.R., Heller, V., Farley, F.J.M., Hearn, G.E. and Rainey, R.C.T., 2012. "Laboratory testing the Anaconda". *Philosophical Transactions of the Royal Society A: Mathematical, Physical and Engineering Sciences*, Vol. 370, pp. 403-424.

Chikazawa, Y., Koshizuka, S. and Oka, Y., 2001. "A particle method for elastic and viscoplastic structures and fluid-structures interactions". *Computational Mechanics*, Vol. 27, pp. 97-106.

Choi, H.I., Park, J.H., Kwon, S.H., Lee, K.H., Lee, S.B. and Yang, Y.J., 2012. "An experimental study on hydro-elasticity in sloshing". In *Proceedings of the 31st International Conference on Ocean, Offshore and Arctic Engineering - OMAE2012*. Rio de Janeiro, Brazil.

Idelsohn, S.R., Marti, J., Limache, A. and Õnate, E., 2008. "Unified lagrangian formulation for elastic solids and incompressible fluids: application to fluid structure interaction problems via the PFEM". *Computer Methods in Applied Mechanics and Engineering*, Vol. 197, pp. 1762-1776.

Koshizuka, S. and Oka, Y., 1996. "Moving particle semi-implicit method for fragmentation of incompressible fluid". *Nuclear Science and Engineering*, Vol. 123, pp. 421-434.

Lugni, C., Bardazzi, A., Faltinsen, O.M. and Graziani, G., 2013. "Hydroelastic challenges for wave-impact phenomena in sloshing flow". In *Proceedings of the 32nd International Conference on Ocean, Offshore and Arctic Engineering - OMAE2013*. Nantes, France.

Mai, T., Hu, Z.Z., Greaves, D. and Raby, A., 2015. "Investigation of hydroelasticity: wave impact on a truncated vertical wall". In *Proceedings of the 25th International Ocean and Polar Engineering Conference - ISOPE2015*. Kona, Hawaii, USA.

Marti, J., Idelsohn, S.R., Limache, A., Calvo, N. and D'Elía, J., 2006. "A fully coupled particle method for quasi-incompressible fluid-hypoelastic structure interactions". *Mecánica Computacional*, Vol. 25, pp. 809-827.

Miras, T., Schotté, J.-S. and Ohayon, R., 2012. "Liquid sloshing damping in an elastic container". *Journal of Applied Mechanics*, Vol. 79.

Rafiee, A. and Thiagarajan, K.P., 2009. "An SPH projection method for simulating fluid-hypoelastic structure interaction". *Computer Methods in Applied Mechanics and Engineering*, Vol. 198, pp. 2785-2795.

Song, M., Koshizuka, S. and Oka, Y., 2003. "Dynamic analysis of elastic solids by MPS method". In *Proceedings of the International Conference on Global Environment and Advanced Nuclear Power Plants - GENES4/ANP2003*. Kyoto, Japan.

Tang, J., Ren, B. and Wang, G., 2016. "Experimental investigation of the three-dimensional sloshing in a square-base tank with elasticity". In *Proceedings of the 12th ISOPE Pacific/Asia Offshore Mechanics Symposium – PACOMS-2016*. Gold Coast, Australia.

Tsukamoto, M.M., Cheng, L.-Y. and Motezuki, F.K., 2016. "Fluid interface detection technique based on neighborhood particles centroid deviation (NPCD) for particle methods". *International Journal for Numerical Methods in Fluids*, Vol. 82, pp. 148-168.

Walhorn, E., Kölke, A., Hübner, B. and Dinkler, D., 2005. "Fluid-structure coupling within a monolithic model involving free surface flows". *Computers and Structures*, Vol. 83, pp. 2100-2111.

Wang, C.M. and Tay, Z.Y., 2011. "Very large floating structures: applications, research and development". In *Proceedings of the 12th East Asia-Pacific Conference on Structural Engineering and Construction — EASEC12*. Hong Kong, China.

Wemmenhove, R., Gladsø, R., Iwanowski, B. and Lefranc, M., 2010. "Comparison of CFD calculations and experiment for the dambreak experiment with one flexible wall". In *Proceedings of the 20th International Offshore and Polar Engineering Conference - ISOPE2010*. Beijing, China.

7. RESPONSIBILITY NOTICE

The authors are the only responsible for the printed material included in this paper.